Int J Adv Manuf Technol (2015) 80:761–774
DOI 10.1007/s00170-015-7029-y

ORIGINAL ARTICLE

Online monitoring of precision optics grinding using acoustic emission based on support vector machine

Dongxu Zhang[1] · **Guo Bi**[1] · **Zhiji Sun**[1] · **Yinbiao Guo**[1]

Received: 14 September 2014 / Accepted: 13 March 2015 / Published online: 3 April 2015

Abstract This paper aims to accomplish online monitoring of precision optics grinding with processing condition factors based on theoretical analysis and through grinding experiments. The model for monitoring surface quality of optical elements online (OSQMM) which contains identification model (IM) and interpolation·factor-support vector regression (*i*•*f*-SVR) is proposed. IM is applied to analyze and determine which kind of processing condition factors and which kind of its feature parameters are the best one to be used for online monitoring. *i*•*f*-SVR which contains the effect factor (*fe*) and interpolation function (I) to overcome the drawbacks of existing SVR models is applied to predict the monitoring thresholds. The grinding experiments were designed and performed. The influences of technological parameters (e.g., grain size of the grinding wheel, grinding depth, speed of the grinding wheel, speed of the worktable, and materials of workpiece) and processing condition factors (e.g., acoustic emission, grinding force, and vibration) on the surface quality were investigated and analyzed by IM. *i*•*f*-SVR was trained and established by the data which were gained through the experiments. After that, the other grinding experiments were performed to apply and verify OSQMM. The results were that the accuracy of alarm for roughness was 85.19 % and the accuracy of alarm for surface shape peak–valley value was 75.93 %. The results show that this method can be effectively applied to monitor the precision optics grinding process online.

✉ Guo Bi
biguoxd@126.com

[1] Department of Mechanical and Electrical Engineering, Xiamen University, Science Building Room 214, Simingnan Road 422, Xiamen 361005, Fujian, China

Keywords Optics grinding · Surface quality · Processing condition factors · Interpolation·factor-support vector regression · Online monitoring

1 Introduction

With the wide application of optics and electronic information technologies in many high-tech sectors (e.g., aerospace, astronomy, national defense, and military), optical elements are being developed with high-precision and free-form surfaces. This has increased the level of accuracy requirement for machining and measurement [1]. Precision grinding is the main machining method for optical elements which can realize high surface quality at high material removal rates [2, 3].

In precision optics grinding, complicated processing technology and manufacturing procedures mean that there are various factors that affect the surface quality in different ways. In addition, the application of the online monitoring technology is very difficult because of the splash of grinding fluid. Now, many studies have focused on processing condition factors such as the acoustic emission signal (AE), grinding force signal (GF), and vibration signal which are given out during the interaction between the grinding wheel and the surface of optical elements [4–7]. Since AE is generated at the moment when the material is dropping from a surface [8], it has been widely applied to the control of the grinding process. Webster et al. [9] determined the relationship between AE, GF, and the material removal rate by extracting and analyzing the AE characteristics to realize surface quality control during the grinding process. Stephenson et al. [10] realized the controlling of the ultra-precision grinding process and recognition of the grinding wheel condition by using AE. Aguiar et al. [11] and Wang et al. [12] used AE to detect grinding wheel wear. Hassui et al. [13] concluded that vibration can be applied to

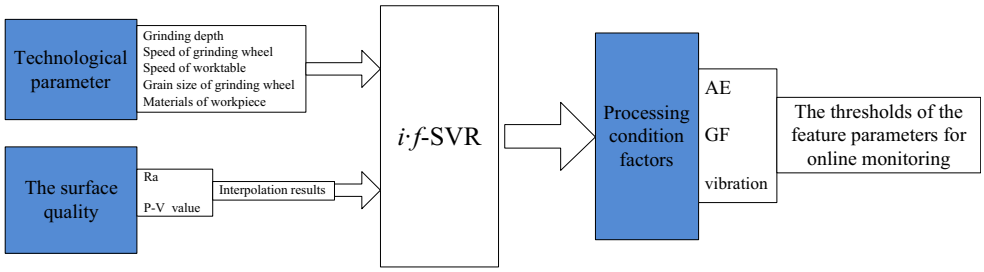

Fig. 1 The structure of *i•f*-SVR

monitor the grinding wheel condition by analyzing the relationship between vibration and the surface quality. Govekar et al. [14] proposed a method that can detect vibration automatically in grinding process in order to avoid the damage of the workpiece. Oliveira et al. [15] studied the effects of environment vibration on the grinding dynamics of the grinding wheel. Kwak et al. [16] used GF to measure the grinding time. Lezanski [17] considered AE, GF, and vibration at the same time to recognize the grinding wheel state in the grinding process.

In the process of monitoring optics grinding with condition factors under the specific technological parameters, machine learning techniques are the main method for solving problems because of the many parameters. Machine learning is an important research field for modern artificial intelligence technology. It realizes data analysis and unknown data prediction through a corresponding mathematical model that is built by studying the training data. Now, neural network and support vector machines (SVMs) are widely applied. Hosokawa et al. [18] used the dynamic spectrum signal of grinding sounds based on a neural network to recognize grinding wheel surface features with better than 80 % accuracy. Chiu et al. [19] established a mathematical model to map the relationship between AE and roughness (Ra) using SVM theory that was able to predict Ra under unknown machining conditions with up to 85 % accuracy. Cho et al. [20] established a damage detection system using SVM theory and were able to identify abnormal conditions during the machining process. Curilem et al. [21] established models for online estimation of the filling level of a semiautogenous mill using both a neural network and a least square-support vector machine and got a good result of energy consumption optimization. Gao et al. [22] put forward a discrete system model and an in-process sensing technique to address the partial removal and precision control for surface grinding with a good experimental result. Liao et al. [23] used hidden Markov model-based clustering method to monitor the condition of grinding wheel and got a useful conclusion.

At present, many advances have been made with regards to monitoring the grinding process to meet the requirements for a precision optics grinding to some extent. However, there are still some shortcomings. Present studies have focused on how Ra is affected by processing conditions, but the surface shape peak–valley (P-V) value, which is another important parameter for the surface quality, is rarely studied. In addition, the method of monitoring grinding process with condition factors has poor real-time performance and cannot realize online monitoring, because it must take some time to make the conclusion for the process after obtaining the condition factors. The model for monitoring surface quality of optical elements online (OSQMM) is proposed to make up the shortcomings.

2 Basic principle of OSQMM

OSQMM is proposed based on SVM theory. At present, several support vector regression (SVR) models have been proposed, such as ε-SVR, ν-SVR, and least-squares SVR since SVMs were proposed by Vapnik in the 1990s [24, 25]. However, these models select the support vectors and calculate the decision function based mainly on the values of the attribute dimension of the input vectors. They cannot balance the degrees of influence of the attribute dimensions on the surface quality of optical elements automatically. In addition, the

Table 1 Technological parameters (control factors) and levels

Factors	Meaning	Level 1	Level 2	Level 3
A	Grain size of grinding wheel (GSGW)	Fine-grained	Medium-grained	–
B	Grinding depth (GD) (μm)	5	10	20
C	Speed of grinding wheel (SGW) (rpm)	900	1200	1500
D	Speed of worktable (SW) (m/min)	3	5	7
E	Materials of workpiece (MW)	JCS1	JCS3	BK7

output vector should be an interval which is obtained by predicting the threshold of condition factors according to the requirement range of surface quality for online monitoring, while the output vector of SVR models that have been proposed has a single attribute dimension in most cases. Thus, existing SVR models cannot be directly applied to online monitoring the surface quality of optical elements in precision grinding process.

Table 2 Experimental design

Serial number of experiment	Factor levels				
	A	B	C	D	E
1	1	1	1	1	1
2	1	2	2	2	2
3	1	3	3	3	3
4	1	1	1	2	3
5	1	2	2	3	1
6	1	3	3	1	2
7	1	1	3	3	2
8	1	2	1	1	3
9	1	3	2	2	1
10	1	1	2	2	1
11	1	2	3	3	2
12	1	3	1	1	3
13	1	1	1	1	2
14	1	2	2	2	3
15	1	3	3	3	1
16	1	1	2	3	3
17	1	2	3	1	1
18	1	3	1	2	2
19	2	1	3	1	1
20	2	2	1	2	2
21	2	3	2	3	3
22	2	1	3	2	3
23	2	2	1	3	1
24	2	3	2	1	2
25	2	1	1	3	1
26	2	2	2	1	2
27	2	3	3	2	3
28	2	1	2	1	3
29	2	2	3	2	1
30	2	3	1	3	2
31	2	1	3	2	2
32	2	2	1	3	3
33	2	3	2	1	1
34	2	1	2	3	2
35	2	2	3	1	3
36	2	3	1	2	1

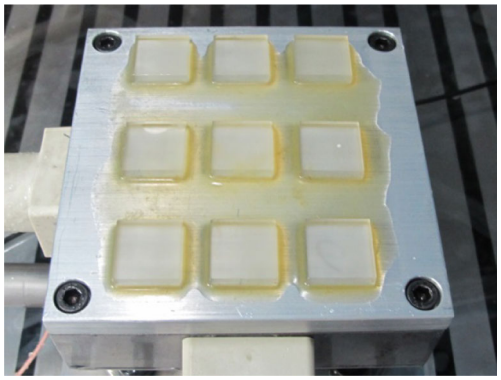

Fig. 2 Optical glass samples

Based on the reasons mentioned above, OSQMM is proposed. In this paper, online monitoring the surface quality is equivalent to online monitoring Ra and P-V value which are used to describe the surface quality. The significance of OSQMM is that the interval of processing condition factors which is used as alarm limits for online monitoring is reverse calculated according to the requirement range of Ra and P-V value. OSQMM is comprised of identification model (IM) and interpolation·factor-support vector regression (*i*•*f*-SVR). IM is applied to identify the correlation between each condition factor and the surface quality in order to determine which condition factor is the best one for online monitoring Ra and P-V value. After that, the relationships of each feature parameter of the condition factor which is determined above and surface quality are quantitatively analyzed to determine which feature parameter is the best one. Then, the thresholds of the feature parameter are calculated by *i*•*f*-SVR.

Three processing condition factors are mainly studied: AE, GF, and vibration. Their feature parameters are studied from the time and frequency domains. IM [26] is used for calculating effect factor (*fe*) to identify the influences of condition

Fig. 3 2MK1760 high-precision grinding machine

Table 3 The details of the grinding machine

Parameters	Value
The range of *x*-axis (mm)	1000
The range of *y*-axis (mm)	500
The range of *z*-axis (mm)	600
The maximum positioning error (μm)	±3
The kind of the grinding wheel	Arc-diamond wheel

Table 4 The details of sensors

The kind of sensor	Value of the sampling frequency (kHz)	Manufacturer	Model
AE	156	Beijing Shenghua Co. Ltd	SAEU2
GF	2	Kistler Co. Ltd	9272
Vibration	1.5	Jiangsu Lianneng Co. Ltd	CA-YD-1107

factors and feature parameters on the surface quality in precision optics grinding.

Figure 1 shows the structure of *i•f*-SVR. Technological parameters and the requirement range of surface quality are the input vectors. The thresholds of the feature parameters in the time or frequency domain of processing condition factors for online monitoring are the output vectors. Interpolation function is proposed to solve the problem that the thresholds cannot be predicted directly because the relationship between the thresholds and the value of surface quality is not linear. The values are calculated with the decision function of *i•f*-SVR and each interpolation value of the requirement range of surface quality. After that, the maximum value and the minimum value are selected as the thresholds.

The hyperplane is established as a decision surface for the decision function of *i•f*-SVR solution. Different types of data are separated by the hyperplane, and the distances between types of data are maximized by the largest interval method. *i•f*-SVR can be expressed as the following optimization problem:

$$\begin{cases} \min\limits_{\omega,b,\xi^{(*)}} \quad \frac{1}{2}\|w\|^2 + C\sum\limits_{i=1}^{l}\left(\xi_i+\xi_i^*\right), \\ s.t. \quad ((w{\cdot}\Phi(x_i{\bullet}fe_i))+b)-y_i \le \varepsilon+\xi_i, \quad i=1,2,\cdots,l \\ \qquad y_i-((w{\cdot}\Phi(x_i{\bullet}fe_i))+b) \le \varepsilon+\xi_i^*, \quad i=1,2,\cdots,l \\ \qquad \xi_i^{(*)} \ge 0, \qquad\qquad i=1,2,\cdots,l \\ x_{i'}^{'} = I(x_{0\min}, x_{0\max}), \quad i'=0,1,\cdots,l' \\ y_{i'}^{'} = w{\cdot}\Phi\left(x_{i'}^{'}\right)+b \quad i'=0,1,\cdots,l' \end{cases} \tag{1}$$

where x is the input vector, fe is the effect factor, w is the adjustable weight vector, b is the bias, C is the penalty parameter, $\xi_i^{(*)}$ is the slack variable used to measure the deviation degree of a data point from model regression under ideal conditions, ε is the translational value of the hyperplane moving up and down along the y-axis, l is the total number of data points, i is the count value, and $\Phi(x)$ is the nonlinear transformation to map x to a higher dimensional feature space. In this paper, a vector with a mark symbol "(*)" in the top right corner stands for two conditions: one is that this vector has "*" in the top right corner and the other is that this vector does not have "*" in the top right corner. x_{0min} is the minimum value of the requirement range of the surface quality, and x_{0max} is the maximum value of the requirement range of the surface quality. I is the interpolation function, $x_{i'}^{'}$ is the result which is calculated by I, i' is the count value of interpolation times, and l' is the total number of interpolation times.

The Lagrange equation of the optimization problem described in Eq. (1) is

$$\begin{aligned} L\left(w,b,\xi^{(*)},\alpha^{(*)},\eta^{(*)}\right) = {} & \frac{1}{2}\|w\|^2 + C\sum_{i=1}^{l}\left(\xi_i+\xi_i^*\right) - \sum_{i=1}^{l}\left(\eta_i\xi_i+\eta_i^*\xi_i^*\right) \\ & -\sum_{i=1}^{l}\alpha_i\left(\varepsilon+\xi_i+y_i-(w{\cdot}\Phi(x_i{\bullet}fe_i))-b\right) \\ & -\sum_{i=1}^{l}\alpha_i^*\left(\varepsilon+\xi_i-y_i+(w{\cdot}\Phi(x_i{\bullet}fe_i))+b\right) \end{aligned} \tag{2}$$

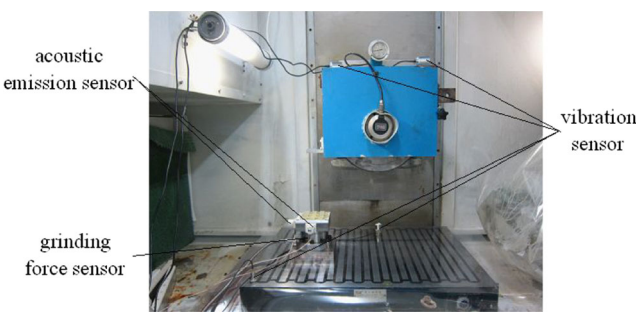

Fig. 4 Installation methods of all sensors and experimental panorama

Fig. 5 Onsite measurement of optical glass samples

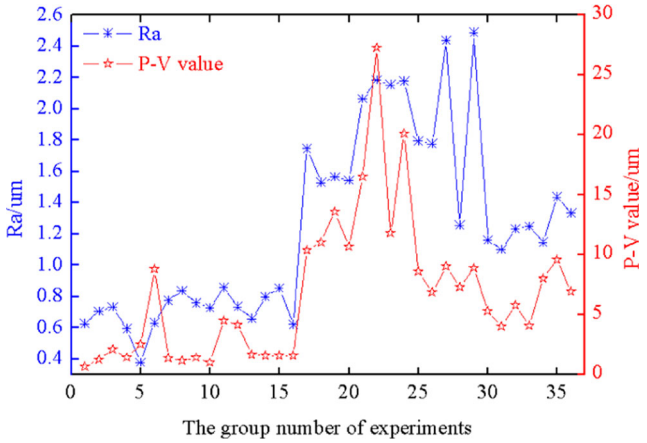

Fig. 6 The measuring results

where $\alpha^{(*)}=(\alpha_1,\alpha_1^*,\ldots,\alpha_l,\alpha_l^*)^{\mathrm{T}}$ and $\eta^{(*)}=(\eta_1,\eta_1^*,\ldots,\eta_l,\eta_l^*)^{\mathrm{T}}$ are the Lagrange multipliers. The optimization equation should satisfy the following equations:

$$\begin{aligned}
&\frac{\partial L}{\partial w}=0 \quad \Rightarrow \quad w=\sum_{i=1}^{l}\left(\alpha_i-\alpha_i^*\right)(x_i\bullet fe_i)\\
&\frac{\partial L}{\partial b}=0 \quad \Rightarrow \quad \sum_{i=1}^{l}\left(\alpha_i-\alpha_i^*\right)=0\\
&\frac{\partial L}{\partial \xi_i}=0 \quad \Rightarrow \quad C-\alpha_i-\eta_i=0\\
&\frac{\partial L}{\partial \xi_i^*}=0 \quad \Rightarrow \quad C-\alpha_i^*-\eta_i^*=0
\end{aligned} \tag{3}$$

The dual form of Eq. (4) is obtained after substituting Eq. (3) into Eq. (2):

$$\begin{aligned}
&\min_{\alpha^{(*)}\in R^{2l}} \ \frac{1}{2}\sum_{i,j=1}^{l}\left(\alpha_i^*-\alpha_i\right)\left(\alpha_j^*-\alpha_j\right)\left(\Phi(x_i\bullet fe_i)\cdot\Phi(x_j\bullet fe_j)\right)\\
&\quad+\varepsilon\sum_{i=1}^{l}\left(\alpha_i^*+\alpha_i\right)-\sum_{i=1}^{l}y_i\left(\alpha_i^*-\alpha_i\right),\\
&s.t. \ \sum_{i=1}^{l}\left(\alpha_i^*-\alpha_i\right)=0,\\
&\quad 0\le\alpha_i{}^{(*)}\le C, \quad i=1,2,\cdots,l
\end{aligned} \tag{4}$$

Equation (5) can be obtained according to the Karush–Kuhn–Tucker (KKT) conditions:

$$\alpha_i\times\alpha_i^*=0 \tag{5}$$

If α_i, which is the component of $\alpha_i^{(*)}$ belonging to (0, C), is chosen, b is solved as follows:

$$\overline{b}=y_j-\left(\overline{\omega}\cdot x_j\bullet fe_j\right)+\varepsilon=y_j-\sum_{i=1}^{l}\left(\overline{\alpha}_i^*-\overline{\alpha}_i\right)\left((x_i\bullet fe_i)\bullet\left(x_j\bullet fe_j\right)\right)+\varepsilon \tag{6}$$

If α_i^*, which is the component of $\alpha_i^{(*)}$ belonging to (0, C), is chosen, b is solved as follows:

$$\overline{b}=y_k-(\overline{\omega}\cdot x_k\bullet fe_k)-\varepsilon=y_k-\sum_{i=1}^{l}\left(\overline{\alpha}_i^*-\overline{\alpha}_i\right)((x_i\bullet fe_i)\bullet(x_k\bullet fe_k))-\varepsilon \tag{7}$$

The value of w is given in Eq. (3). Thus, the decision function of *i•f*-SVR is as follows:

$$y=g(x\bullet fe)=\sum_{i=1}^{l}\left(\alpha_i^*-\alpha_i\right)K((x\bullet fe),(x_i\bullet fe_i))+b \tag{8}$$

where $K((x\bullet fe),(x_i\bullet fe_i))=(\Phi(x_i\bullet fe_i)\cdot\Phi(x\bullet fe))$ is the kernel function that meets the Mercer theorem. The RBF was used in this study, as shown in Eq. (9), because of its many advantages, such as a simple expression, few kernel parameters, good smoothness, and fast computing speed.

$$K((x\bullet fe),(x_i\bullet fe_i))=\exp\left(\frac{1}{\sigma^2}\left\|(x\bullet fe)-(x_i\bullet fe_i)\right\|^2\right) \tag{9}$$

The interpolation function I is shown in Eq. (10) that

$$\begin{cases} I(x_{0\min},x_{0\max})=x_{0\min}+[\lambda\bullet(x_{0\max}-x_{0\min})]\bullet i', & i'=0,1,\cdots l'\\ \lambda \quad\bullet\quad l' \quad=\quad 1 \end{cases} \tag{10}$$

Where x_{0min}, x_{0max}, $x_{i'}$, i', and l' are defined as above, and λ whose interval is (0,1) is interpolation factor in order to determine the interpolation value.

Table 5 Features extracted from each processing condition factor

Kinds of signals	Kinds of features					
	Time domain			Frequency domain		
Acoustic emission	Root mean square (RMS)	Skewness index	Peak factor	Centroid frequency	Frequency variance	Mean square frequency (MSF)
Vibration	RMS	Skewness index	Peak factor	Centroid frequency	Frequency variance	MSF
Grinding force	Average value in X direction (A-X)	A-Y	A-Z	–	–	–

Fig. 7 Feature values

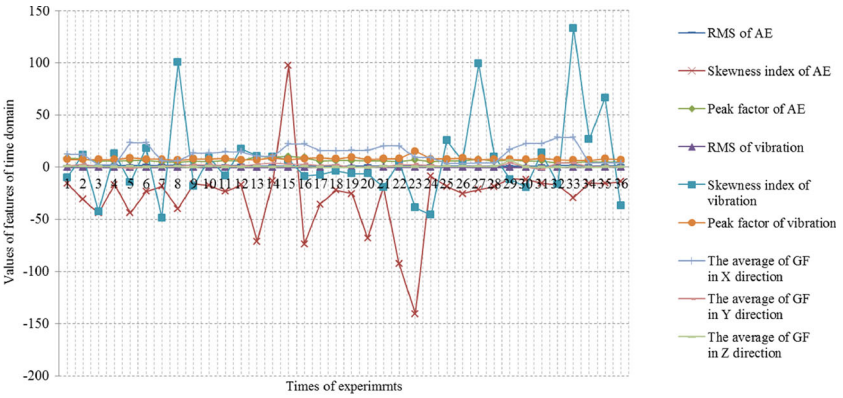

(a) Time domain

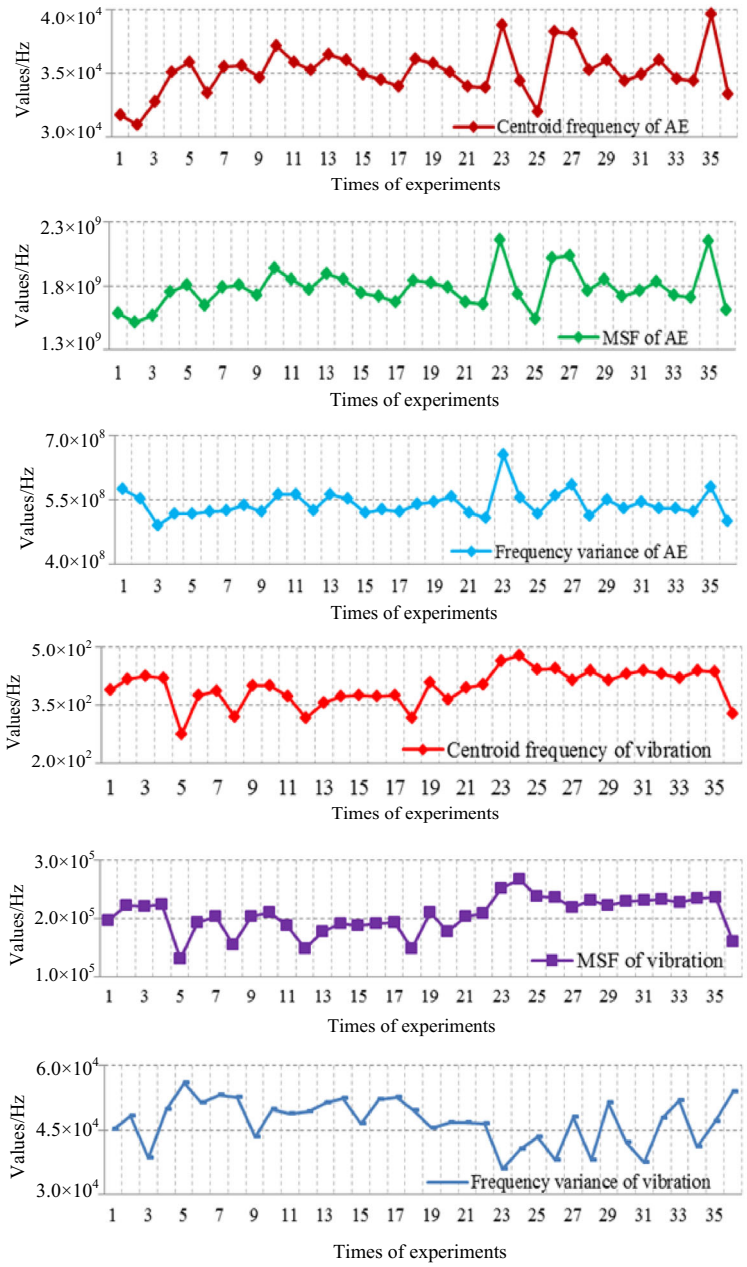

(b) Frequency domain

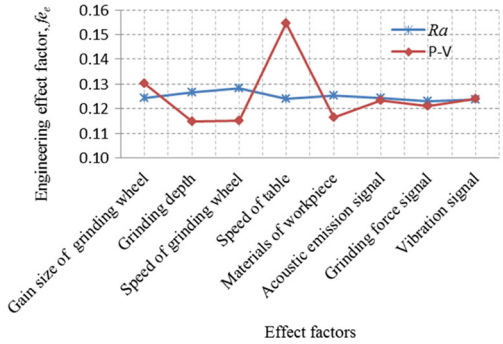

Fig. 8 Calculation results of *fe*

3 Experiments and discussion

3.1 Solve the decision function of *i•f*-SVR and calculate *fe*

The experiments were performed to obtain training data in order to solve the decision function of *i•f*-SVR and calculate *fe*. The Taguchi method was adopted to design the experiments to consider both the influence of a single factor and the cross-effects of several factors on the surface quality. The Taguchi method is a powerful tool that uses an orthogonal table to arrange experiments in order to realize equilibrium dispersion. Thus, the whole parameter space can be studied with the minimum number of experiments. This method is a simple and scientific design method that greatly reduces the experimental time to build models for response functions compared with traditional experimental methods [27, 28].

3.1.1 Experimental design

Five technological parameters (control factors) were examined in the experiments: the grinding depth, speed of the grinding wheel, speed of the worktable, grain size of the grinding wheel, and materials of the workpiece. Two levels of grain size and three levels of each of the other four control factors were selected according to the characteristics of the optics grinding. Table 1 lists the specific values.

A L_{36} ($2^{11}\times3^{12}$) orthogonal array was chosen according to the number of control factors and levels of each factor, as shown in Table 2. This array has 36 rows corresponding to the experiment times. It can accommodate 23 control factors at most; 11 control factors have two levels, whereas the remaining 12 control factors have three levels. This array requires 35 degrees of freedom (DOFs). In the experiments, the grain size of the grinding wheel (factor A) had 1 DOF, and the rest of the four factors had eight ($4\times(3-1)$) DOFs. The interaction between the grain size (factor A) and grinding depth (factor B) and the interactions among the grinding depth (factor B), speed of the grinding wheel (factor C), speed of the worktable (factor D), and materials of the workpiece (factor E) were needed to study according to the characteristics of the precision optics grinding. The DOFs were $26((2-1)\times(3-1)+6\times(3-1)\times(3-1))$. Thus, a total of 35 DOFs was required in the experiments. Because the total number of DOFs of the orthogonal array must be more than or equal to that of the experiments required by the Taguchi method, the L_{36} ($2^{11}\times3^{12}$) orthogonal array was chosen.

3.1.2 Experimental conditions and measurement

Each experiment was performed on three optical glass samples (the three samples were called an optical glass sample group), as shown in Fig. 2, so three sets of data were obtained for each experiment. This method effectively avoids the interference of random error and ensures the authenticity of the data. Three optical glass sample groups for three experiments were pasted on one piece of aluminum sheet by superglue. Each aluminum sheet was 120×120 mm in size, and each optical glass sample was 20×20×3 mm. The spacing in the transverse direction was 10 mm, whereas the spacing in the longitudinal direction was 20 mm. The transverse edge distance was 20 mm, and the longitudinal edge distance was 10 mm.

The experiments were performed using a 2MK1760 high-precision grinding machine shown in Fig. 3, of which the parameters were listed in Table 3. The P-V value of 430×430 mm aspheric optics ground on this machine was 3–5 μm, and Ra was within 0.1 μm.

In the experiments, AE, GF, and vibration were measured with sensors, of which the installation method was shown in Fig. 4 and the details were listed in Table 4.

After three experiments, every optical glass sample was measured onsite, as shown in Fig. 5, which eliminated the repetitive positioning error of the workpiece. The measuring tool was a noncontact laser displacement sensor (Keyence). Figure 6 showed the measuring results.

Table 6 Features extracted from AE

	Feature parameters of AE					
Time domain features	RMS	Skewness index	Peak factor	Peakedness coefficient	Margin index	Ring-down count rate
Frequency domain features	MSF	Signal energy	Centroid frequency	Frequency variance	–	–

Fig. 9 The predicted results

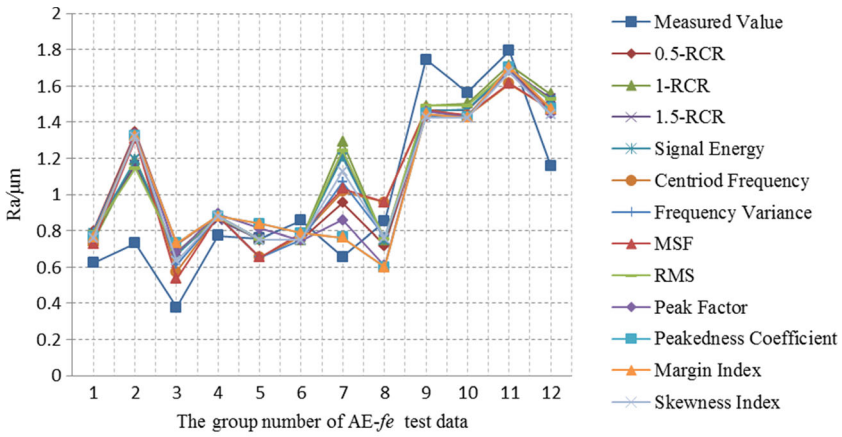

(a) the predicted results of Ra

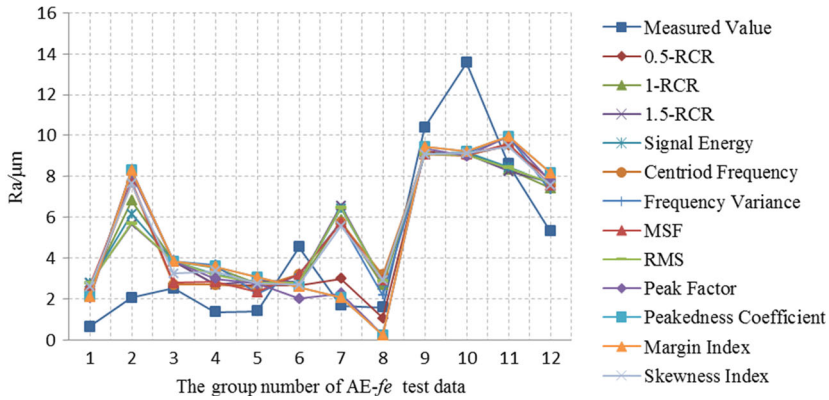

(b) the predicted results of P-V value

3.1.3 Feature extraction of processing condition factors

The variation law of optics grinding is difficult to determine directly from the original signals collected by each sensor because these signals contain redundant information and have strong randomness. In addition, the signals are often described in the time and frequency domains. In this study, fast Fourier transform (FFT) was used to change the original signals from the time domain to the frequency domain.

Many features describe a signal in the time and frequency domains. Table 5 lists the features used in this study considering both the precision optics grinding characteristics and the signal features [29]. Figure 7 shows the values in the (a) time domain and (b) frequency domain.

3.1.4 Calculate fe of the processing condition factors

fe of the technological parameters and the processing condition factors was calculated by IM with the data obtained from the experiments above, as shown in Fig. 8 [26].

The conclusion that AE should be used for online monitoring Ra and vibration should be used for online monitoring P-V value is obtained from *fe*. However, the grinding process will be affected in the case of two or more than two kinds of sensors installed on the grinding machine in actual grinding process, especially for large-aperture optics. In addition, though the correlation between vibration and P-V value is more significant than that between AE and P-V value, the difference is small. AE is selected for online monitoring surface quality.

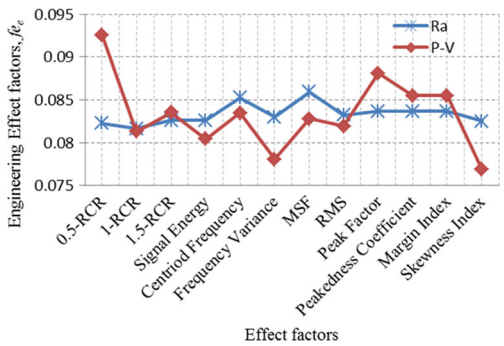

Fig. 10 Calculation results of *fe* for each feature parameter

Table 7 Parameters of experiment 2

Class	GSGW	SGW (rpm)	SW (m/min)	GD (μm)	MW	Group number	The count of group number
1	Fine-grained	1500	5	2	BK7	3	1–3
2	Medium-grained	1500	5	20	JCS3	4	4–7
3	Medium-grained	1500	5	20	K9	2	8–9
4	Medium-grained	1500	5	30	JCS1	2	10–11
5	Medium-grained	1500	5	30	JCS3	2	12–13
6	Medium-grained	1500	5	30	K9	2	14–15
7	Fine-grained	1500	5	5	JCS1	2	16–17
8	Fine-grained	1500	5	5	JCS3	3	18–20
9	Fine-grained	1500	5	20	BK7	2	21–22
10	Fine-grained	1500	5	5	BK7	3	23–25
11	Fine-grained	1500	7	5	BK7	4	26–29
12	Fine-grained	1500	7	20	BK7	4	30–32
13	Fine-grained	1500	5	3	BK7	16	33–48
14	Fine-grained	900	5	5	BK7	3	49–51
15	Medium-grained	1500	7	20	BK7	4	52–54

3.1.5 Calculate fe of the AE feature parameters

It will lose its meaning that many feature parameters need be calculated in the case of online monitoring, because it slows the calculation speed a lot. IM is applied to find which kind of feature parameter of AE has the most significant correlation with surface quality. Several kinds of feature parameters were added on the basis of the experiments above in order to have more practicability, as shown in Table 6.

The measurement data gained from the experiments above were taken as the AE-*fe* training data, and the AE-*fe* test data comprised 12 groups of data that were selected isometrically from the AE-*fe* training data. Figure 9 shows the predicted results for (a) Ra and (b) the P-V value. In the figure, each curve marked with a factor's name shows the results predicted by the decision function of *i•f*-SVR that was trained and established by this factor. *fe* of each feature parameter which was listed in Table 6 was then calculated, as shown in Fig. 10. MSF has the strongest correlate degree with Ra, and ring-down count rate with threshold 0.5 (0.5-RCR) has the strongest correlate degree with P-V value. So, MSF is selected for online monitoring Ra, and 0.5-RCR is selected for online monitoring P-V value.

3.1.6 Train and establish i•f-SVR

The measurement data gained from the experiments were taken as the training data. The five technological parameters and the requirement range of Ra and P-V value were the input vectors. The thresholds of MSF and 0.5-RCR of AE were the output vectors. *i•f*-SVR was trained and established to be used for online monitoring.

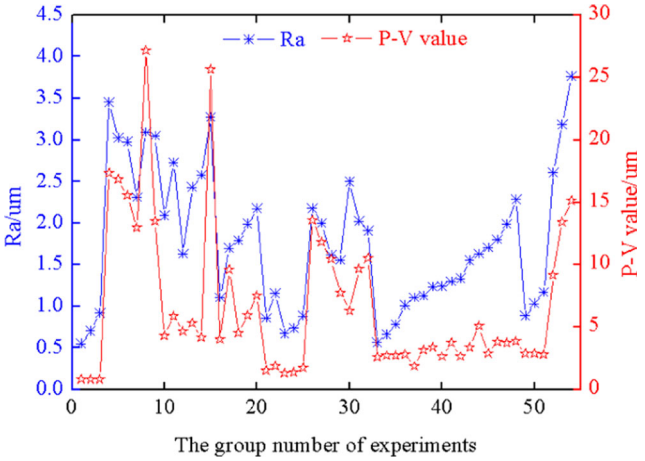

Fig. 11 The measuring results of Ra and P-V value

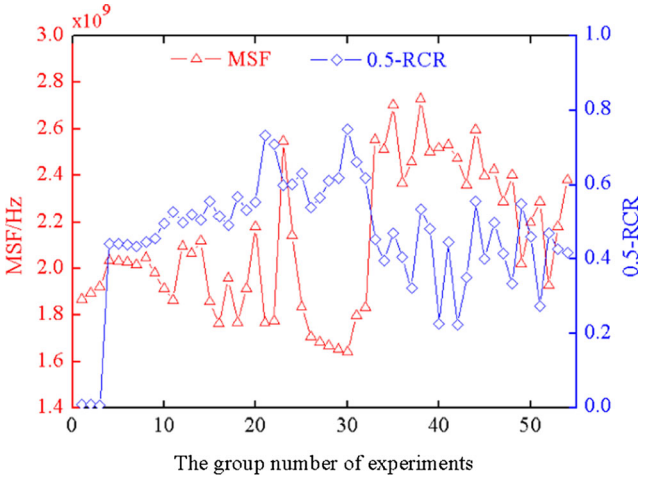

Fig. 12 The measuring results of MSF and 0.5-RCR

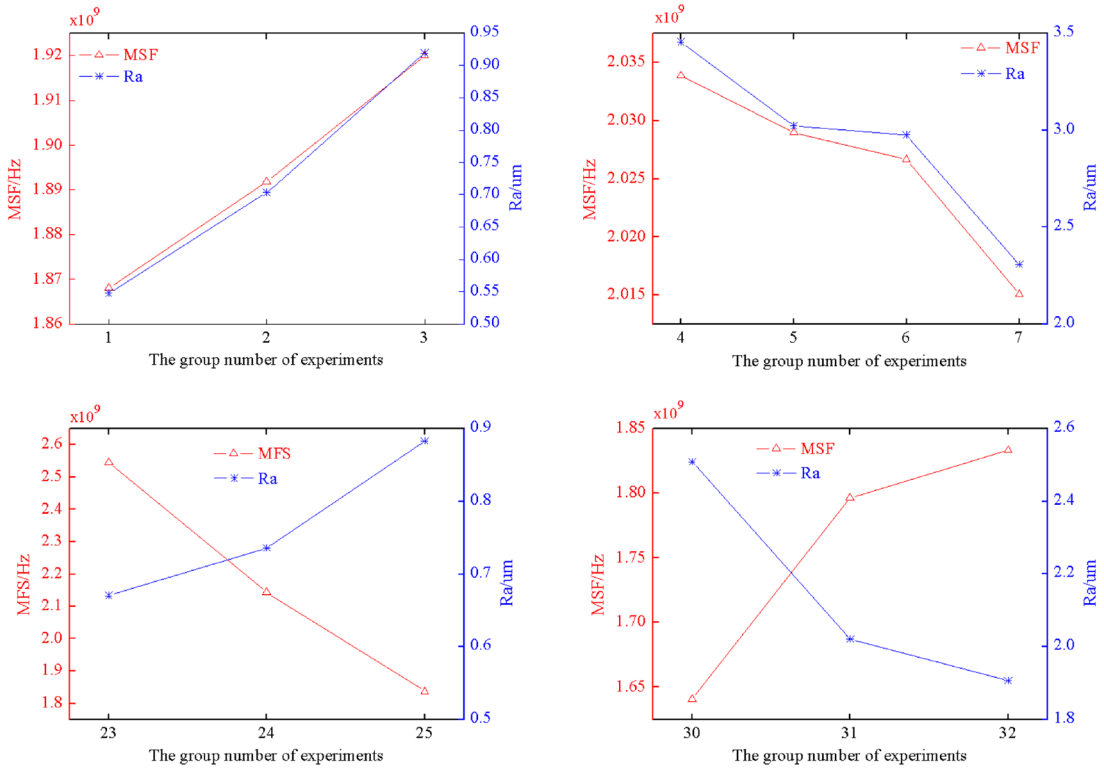

(a) The relationship curve between MSF and Ra

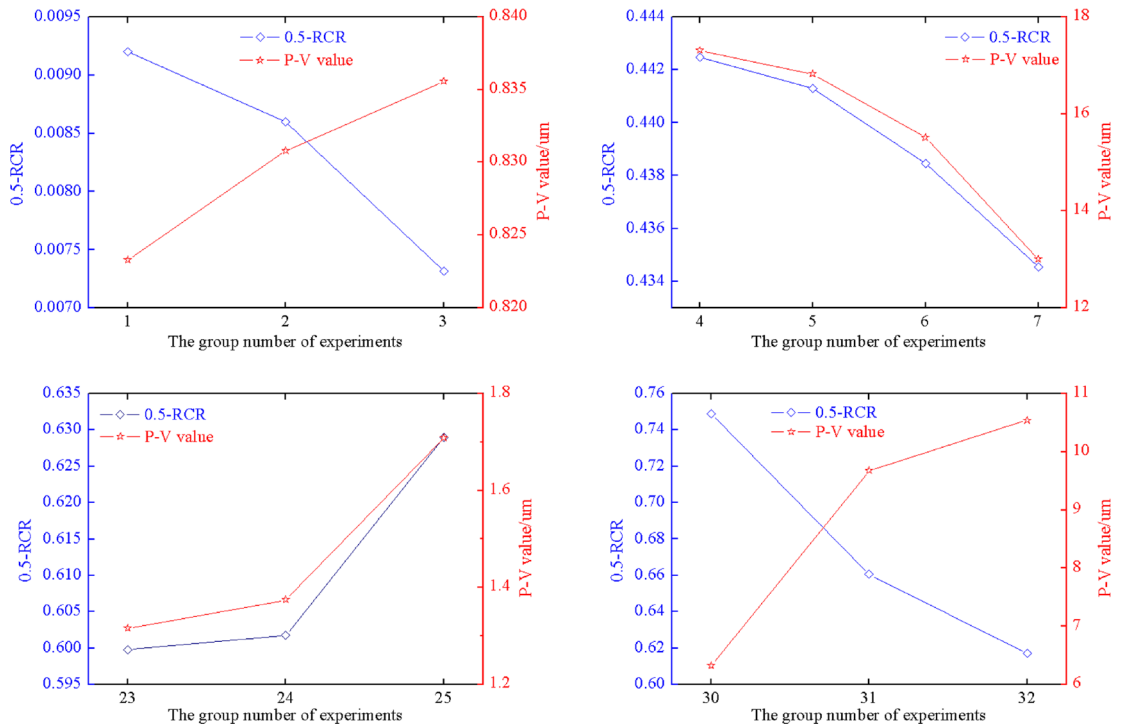

(b) The relationship curve between 0.5-RCR and P-V value

Fig. 13 The relationship between the feature parameter and surface quality

3.2 Application and verification of OSQMM

3.2.1 Experimental design

The experiments were performed to apply and verify the effectiveness of OSQMM. The value of five technological parameters and the requirement range of the surface quality were selected according to the actual grinding process, as shown in Table 7. Several pieces of optical glass samples were ground on condition of each group of technological parameters. The data obtained by grinding a piece of glass sample is called a group of data, and the data obtained by grinding several pieces of glass samples in the same technological parameters is called a class of data in this study. There were 15 classes of data, that is to say 54 groups of data were obtained from the experiments. The experimental conditions and the measuring method were the same as that in 3.1.2 section. Figure 11 shows the measuring results of Ra and P-V value, and Fig. 12 shows the measuring results of MSF and 0.5-RCR.

3.2.2 Data analysis

Figure 13 is drawn with part of the original data. The relationship between MSF and Ra representation is shown by (a), and the relationship between 0.5-RCR and P-V value representation is shown by (b). MSF of AE has significant correlation with Ra. There is a positive or negative correlation between MSF and Ra along with the different technological

Table 8 The thresholds

Class	The requirement range of surface quality after grinding		The thresholds for online monitoring	
	Ra (μm)	P-V value (μm)	MSF	0.5-RCR
1	[0.5, 1.0]	[0, 5]	[1854165256, 1922612663]	[0.0054, 0.0114]
2	[2.0, 2.5]	[10, 15]	[2010643343, 2019319508]	[0.4311, 0.4411]
	[2.5, 3.0]	[15, 20]	[2018207308, 2030807811]	[0.4401, 0.4473]
	[3.0, 3.5]		[2031705601, 2041202676]	
3	[3.0, 3.5]	[10, 15]	[1962667681, 2044355584]	[0.4506, 0.4621]
		[25, 30]		[0.4405, 0.4466]
4	[2.0, 2.5]	[0, 5]	[1883577727, 1912446300]	[0.4937, 0.5086]
	[2.5, 3.0]	[5, 10]	[1845944783, 1872467727]	[0.5086, 0.5305]
5	[1.5, 2.0]	[0, 5]	[2085897876, 2117701505]	[0.4907, 0.5102]
	[2.0, 2.5]	[5, 10]	[2043747429, 2075792886]	[0.5033, 0.5225]
6	[2.5, 3.0]	[0, 5]	[1937343742, 2116434747]	[0.5015, 0.5055]
	[3.0, 3.5]	[25, 30]	[1719349429, 1939123742]	[0.5516, 0.5653]
7	[1.0, 1.5]	[0, 5]	[1760770206, 1886851234]	[0.5086, 0.5327]
	[1.5, 2.0]	[5, 10]	[1874870435, 2223377558]	[0.4865, 0.5086]
8	[1.5, 2.0]	[0, 5]	[1525510252, 1932965466]	[0.5586, 0.5703]
	[2.0, 2.5]	[5, 10]	[1932965466, 2233601145]	[0.5284, 0.5586]
9	[0.5, 1.0]	[0, 5]	[1739629652, 1780108215]	[0.7037, 0.7334]
	[1.0, 1.5]		[1772508616, 1805326562]	
10	[0.5, 1.0]	[0, 5]	[1775535346, 2594866767]	[0.5970, 0.6305]
11	[1.5, 2.0]	[5, 10]	[1650469588, 1700030453]	[0.5881, 0.6248]
	[2.0, 2.5]	[10, 15]	[1700030453, 1732800280]	[0.5349, 0.5771]
12	[1.5, 2.0]	[5, 10]	[1798045435, 1905867177]	[0.6434, 0.7498]
	[2.0, 2.5]	[10, 15]	[1638637705, 1787000035]	[0.5531, 0.6247]
13	[0.5, 1.0]	[0, 5]	[2510063602, 2565469515]	[0.3777, 0.4576]
	[1.0, 1.5]	[5, 10]	[2414397870, 2518011222]	[0.4606, 0.3973]
	[1.5, 2.0]		[2241811287, 2414397870]	
	[2.0, 2.5]		[2026830025, 2341511787]	
14	[0.5, 1.0]	[0, 5]	[1630791641, 2190000068]	[0.1910, 0.8544]
	[1.0, 1.5]		[2192322984, 2350247616]	
15	[2.5, 3.0]	[5, 10]	[1878537488, 2077139815]	[0.4500, 0.4702]
	[3.0, 3.5]	[10, 15]	[2088149905, 2260467524]	[0.4233, 0.4449]
	[3.5, 4.0]	[15, 20]	[2259469466, 2388644417]	[0.4071, 0.4233]

parameters. 0.5-RCR of AE has significant correlation with P-V value. There is a positive or negative correlation between 0.5-RCR and P-V value along with the different technological parameters.

The threshold of each class of data was calculated by *i•f*-SVR. The interval was divided per 0.5 μm to calculate the threshold for online monitoring Ra, and the interval was divided per 5 μm to calculate the threshold for online monitoring P-V value. The interpolation was performed between x_{0min} and x_{0max} according to Eq. (10) on condition that λ equaled 0.2. The feature parameters corresponding each interpolation value were then solved. After that, the maximum value and the minimum value are selected as the thresholds. Table 8 lists the thresholds of each class of data, and Fig. 14 shows the comparison results between the thresholds and measured values.

There were 46 groups of data whose the measured values of MSF belonged to the thresholds in all the 54 groups of data. So, the accuracy rate was 85.19 %. There were 42 groups of data whose measured values of 0.5-RCR belonged to the thresholds in all the 54 groups of data. So, the accuracy rate was 77.78 %.

4 Discussion

It is the prerequisite that Ra and P-V value have the homodromous or reverse variation, in other words, Ra and P-V value cannot have the random variation, as shown in Fig. 15a. Under this prerequisite, MSF and Ra, 0.5-RCR, and P-V value have the significant correlation. Without the prerequisite, the correlation is poor, as shown in Fig. 15b, c. Calculating the thresholds by *i•f*-SVR also required the prerequisite. The accuracy rate of online monitoring Ra was 97.37 % on condition that it was the homodromous or reverse variation between Ra and P-V value, while the accuracy rate was just 56.25 % on condition that it was the random variation between Ra and P-V value (the 13th class data of experiment 2). The same conclusion can be drawn for online monitoring P-V value. The accuracy rate was 94.74 % under the prerequisite, while the accuracy rate was just 31.25 %.

In actual precision optics grinding, the preprocessing for the surface of optical elements is needed to avoid the harmful effects caused by local jump of the blank. Because Ra and P-V value will have the homodromous or reverse variation after preprocessing, OSQMM can be effectively applied to online monitor the precision optics grinding process.

5 Conclusion

The proposed mathematic model was used to monitor grinding process online by combining SVM theory with experiments. It has realized giving feedback of the present states of optical elements real-timely by using the processing condition

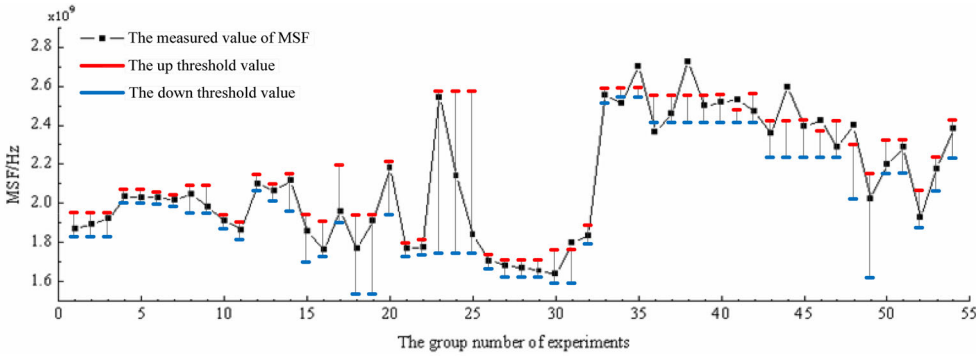

(a) Error band for on-line monitoring Ra

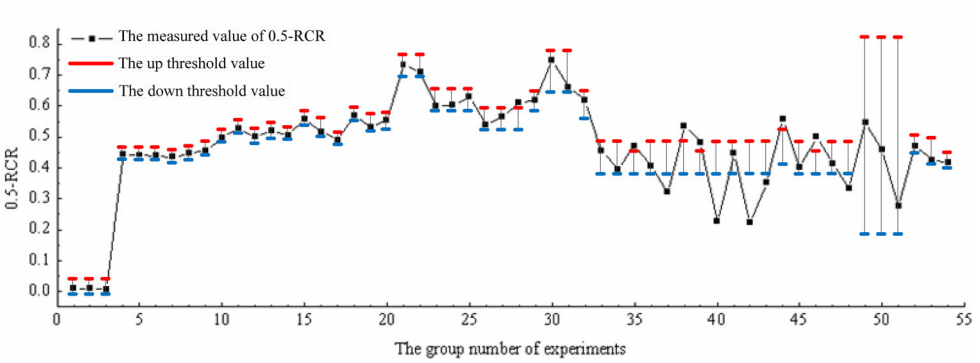

(b) Error band for on-line monitoring P-V value

Fig. 14 Calculation results of thresholds

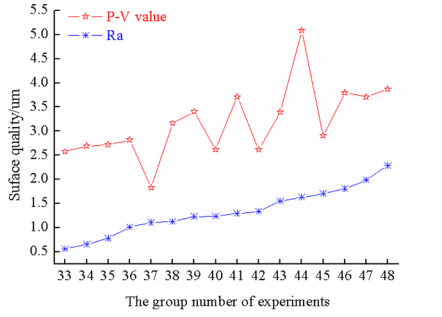

(a) The random variation curve between Ra and P-V value

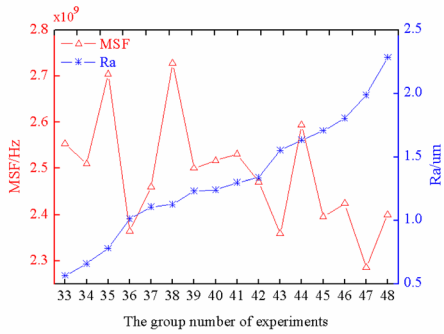

(b) The variation curve between MSF and Ra

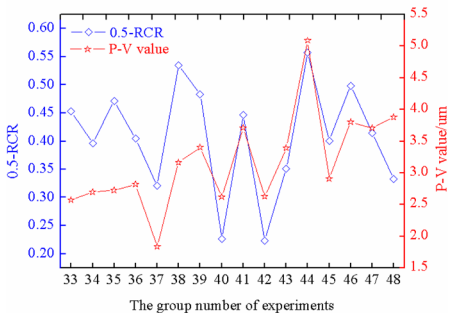

(c) The variation curve between 0.5-RCR and P-V value

Fig. 15 The relationship of the feature parameter and the surface quality under the random variation between Ra and P-V value

factors. The influences of the processing condition factors on the surface quality were quantitatively analyzed. The following conclusions were obtained:

1. *i•f*-SVR overcomes the disadvantages of existing SVR models that have been applied to monitor precision optics grinding online. *fe* and I were introduced.
2. On condition that Ra and P-V value had homodromous or reverse variation, MSF of AE had significant correlation with Ra, and 0.5-RCR of AE had significant correlation with P-V value.
3. The experiments which used *i•f*-SVR for online monitoring were performed. The results show that the accuracy rate was 85.19 % for Ra, and the accuracy rate was 75.93 %. On condition that Ra and P-V value had homodromous or reverse variation, the results of online monitoring were much better. The accuracy rate was 97.37 % for Ra, and the accuracy rate was 94.74 %. OSQMM can be effectively applied to monitor the precision optics grinding process online.

Acknowledgments This work was financially supported by LPMT, CAEP (No. KF13011), and the National Natural Science Funds of China (No. 51075343).

Compliance with Ethical Standards

1. The material has not been published in whole or in part elsewhere.
2. The paper is not currently being considered for publication elsewhere.
3. All authors have been personally and actively involved in substantive work leading to the report and will hold themselves jointly and individually responsible for its content.
4. All relevant ethical safeguards have been met in relation to patient or subject protection or animal experimentation.

References

1. Pollicove HM (2000) Next generation optics manufacturing technologies. Proc SPIE Adv Opt Manuf Test Technol 4231:8–15
2. Han XS, Wu TY (2013) Analysis of acoustic emission in precision and high-efficiency grinding technology. Int J Adv Manuf Technol 67:1997–2006
3. Liao TW, Ting CF, Qu J, Blau PJ (2006) A wavelet-based methodology for grinding wheel condition monitoring. J Mach Tool Manuf 47:580–592
4. Liang SY, Hecker RL, Landers RG (2004) Machining process monitoring and control: the-state-of-the-art. J Manuf Sci Eng 126(5): 297–310
5. Xu LM, Shi L, Zhao XM (2008) Monitoring and compensation of thermal error of profile grinding spindle. Adv Grinding Abras Technol 14(359–360):219–223
6. Franco-Gasca LA, Romero-Troncoso RJ, Herrera-Ruiz G, Peniche-Vera RR (2009) FPGA based failure monitoring system for machining processes. Int J Adv Manuf Technol 40:676–686
7. Wegener K, Hoffmeister HW, Karpuschewski B, Kuster F, Hahmann WC, Rabiey M (2011) Conditioning and monitoring of grinding wheels. CIRP Ann Manuf Technol 60:757–777
8. Liu Q, Chen X, Gindy N (2006) Investigation of acoustic emission signals under a simulative environment of grinding burn. Int J Mach Tools Manuf 46:284–292
9. Webster J, Marinescu I, Bennett R (1994) Acoustic emission for process control and monitoring of surface integrity during gringing. Ann CIRP 43(1):299–304
10. Stephenson DJ, Sun X, Zervos C (2006) A study on ELID ultra precision grinding of optical glass with acoustic emission. Int J Mach Tool Manuf 46:1053–1063
11. Aguiar PR, Oliveira JFG (1999) Production grinding burn detection using acoustic emission and electric power signals. Abrasives 8pp
12. Wang Z, Willett P, Deaguiar PR, Webster J (2001) Neural network detection of grinding burn from acoustic emission. Int J Mach Tool Manuf 41(2):283–309
13. Hassui A, Diniz AE (2003) Correlating surface roughness and vibration on plunge cylindrical grinding of steel. Int J Mach Tool Manuf 43:855–862

14. Govekar E, Baus A, Gradisek J, Klocke F, Grabec I (2002) A new method for chatter detection in grinding. CIRP Ann Manuf Technol 51(1):267–270
15. Oliveira JFG, Franca TV, Wang JP (2008) Experimental analysis of wheel/workpiece dynamic interactions in grinding. CIRP Ann Manuf Technol 57(1):329–332
16. Kwak JS, Ha MK (2004) Detection of dressing time using the grinding force signal based on the discrete wavelet decomposition. Int J Adv Manuf Technol 23:87–92
17. Lezanski P (2004) An intelligent system for grinding wheel condition monitoring. J Mater Process Technol 109:258–263
18. Hosokawa A, Mashimo K, Yamada K, Ueda T (2004) Evaluation of grinding wheel surface by means of grinding sound discrimination. JSME Int J Ser C 47(1):52–58
19. Chiu NH, Guao YY (2008) State classification of CBN grinding with support vector machine. J Mater Process Technol 201:601–605
20. Cho S, Asfour S, Onar A, Kaundinya N (2005) Tool breakage detection using support vector machine learning in a milling process. Int J Mach Tool Manuf 45:241–249
21. Curilem M, Acuna G, Cubillos F, Vyhmeister E (2011) Neural networks and support vector machine models applied to energy consumption optimization in semiautogeneous grinding. Chem Eng Trans 25:761–766
22. Gao Y, Huang X, Zhang Y (2010) An improved discrete system model for form error control in surface grinding. J Mater Process Technol 210:1794–1804
23. Liao TW, Hua GG, Qu J, Blau PJ (2006) Grinding wheel condition monitoring with hidden markov model-based clustering methods. Mach Sci Technol 10:511–538
24. Vapnik VN (1995) The nature of statistical learning theory. Springer, New York
25. Deng NY, Tian YJ (2009) Support vector machines—theory, algorithm and expanding. Science press, Beijing
26. Zhang DX, Yang P, Zhang YT, Bi G, Guo YB (2015) Influences analysis of processing factors on surface quality in optics grinding based on ε-support vector regression. Proc Inst Mech Eng C J Mech Eng Sci (accepted)
27. Ross PJ (1996) Taguchi techniques for quality engineering. McGraw-Hill, New York
28. Antony J, Perry D, Wang CB, Kumar M (2006) An application of Taguchi method of experimental design for new product design and development process. Assem Autom 26(1):18–24
29. Chen HT (2013) Study on tool wear monitoring and prediction technology based on multi-parameter information fusion. Southwest Jiaotong University, Chengdu